PAPER

The features of the global GAM in OH and ECRH plasmas in the T-10 tokamak

IOP Publishing | International Atomic Energy Agency Nuclear Fusion
Nucl. Fusion **55** (2015) 063001 (8pp) doi:10.1088/0029-5515/55/6/063001

The features of the global GAM in OH and ECRH plasmas in the T-10 tokamak

A.V. Melnikov[1,2], L.G. Eliseev[1], S.V. Perfilov[1], S.E. Lysenko[1], R.V. Shurygin[1], V.N. Zenin[1], S.A. Grashin[1], L.I. Krupnik[3], A.S. Kozachek[3], R.Yu. Solomatin[1], A.G. Elfimov[4], A.I. Smolyakov[1,5], M.V. Ufimtsev[6] and The HIBP Team[3]

[1] National Research Centre 'Kurchatov Institute', Moscow, Russia
[2] Department of Plasma Physics, National Research Nuclear University MEPhI, Moscow, Russia
[3] Institute of Plasma Physics, Kharkov Institute of Physics and Technology, Kharkov, Ukraine
[4] Institute of Physics, University of São Paulo, São Paulo, Brazil
[5] University of Saskatchewan, 116 Science Place, Saskatoon, Canada
[6] Faculty of Computational Mathematics and Cybernetics, Lomonosov Moscow State University, Moscow, Russia

E-mail: melnikov_07@yahoo.com

Received 22 December 2014, revised 13 March 2015
Accepted for publication 23 March 2015
Published 30 April 2015

Abstract

Zonal flows and their high-frequency counterpart, the geodesic acoustic modes (GAMs) are considered as a possible mechanism of the plasma turbulence self-regulation. In the T-10 tokamak GAMs have been studied by the heavy ion beam probing and multipin Langmuir probes. The wide range of the regimes with Ohmic, on-axis and off-axis electron cyclotron resonance heating (ECRH) were studied ($B_t = 1.5$–2.4 T, $I_p = 140$–300 kA, $\bar{n}_e = (0.6$–$6.0) \times 10^{19}$ m^{-3}, $P_{EC} < 1.2$ MW). It was shown that GAM has radially homogeneous structure and poloidal $m = 0$ for potential perturbations. The local theory predicts that $f_{GAM} \sim \sqrt{T/m_i}/R$, that means the frequency increases with the decrease of the minor radius. In contrast, the radial distribution of experimental frequency of the plasma potential and density oscillations, associated to GAM, is almost uniform over the whole plasma radius, suggesting the features of the nonlocal (global) eigenmodes. The GAM amplitude in the plasma potential also tends to be uniform along the radius. GAMs are more pronounced during ECRH, when the typical frequencies are seen in the narrow band from 22 to 27 kHz for the main peak and 25–30 kHz for the higher frequency satellite. GAM characteristics and the range of GAM existence are presented as functions of T_e, density, magnetic field and P_{EC}.

Keywords: geodesic acoustic modes, tokamak, heavy ion beam probing

(Some figures may appear in colour only in the online journal)

1. Introduction

In the recent years there has been significant interest in tokamak plasma fluctuations that exhibit scaling with geodesic acoustic frequency $f_{GAM} \sim \sqrt{T/m_i}/R$. Geodesic acoustic modes (GAMs) being the high-frequency counterpart of zonal flows, have been intensively studied as a possible mechanism of the plasma turbulence self-regulation [1]. GAMs involving $m = 0$ component of the electrostatic potential and $m = 1$ component of the plasma pressure were first introduced in [2] within the ideal magnetohydrodynamic (MHD) model. It has been realized recently that both GAM and beta induced Alfvén Eigenmodes (BAEs), having low, but not zero poloidal m and toroidal n numbers in potential perturbation [3], may have the same frequency given by the expression:

$$f_{GAM/BAE} = \frac{V_{Ti}}{2\pi R} \times \sqrt{\frac{7}{4} + \tau_e + q^{-2}\left(\frac{23}{2} + 8\tau_e + 2\tau_e^2\right)(7 + 4\tau_e)^{-1}}, \quad (1)$$

where $\tau_e = T_e/T_i$, $V_{Ti}^2 = 2T_i/m_i$ [4, 5]. In toroidal geometry, the perturbations of ion pressure due to toroidal compressibility are anisotropic resulting in the net adiabatic index of 7/4 [6]. The second term in (1) is related to electron compressibility (note that the perturbation of the electron and ion pressure occurs at the $m = 1$ sideband). The terms with q^{-2} are due to parallel compressibility of ions and electrons resulting in ion sound modes at the first harmonic. The expression (1) describes the local (continuum) spectrum, in which the local $f_{GAM/BAE}$ changes with radius due to the variation of T_e, T_i and q as functions of $\rho = r/a$. There are some experimental works showing the radial variation of the GAM frequency [7]. However, other experiments suggest that the observed GAM fluctuations have constant frequency over some radial extent, limited by diagnostic capabilities, and thus differ from (1) [8–11]. So, the GAM radial structure is an open question at the moment.

In the T-10 tokamak the modes in the geodesic acoustic frequency range have been studied by the heavy ion

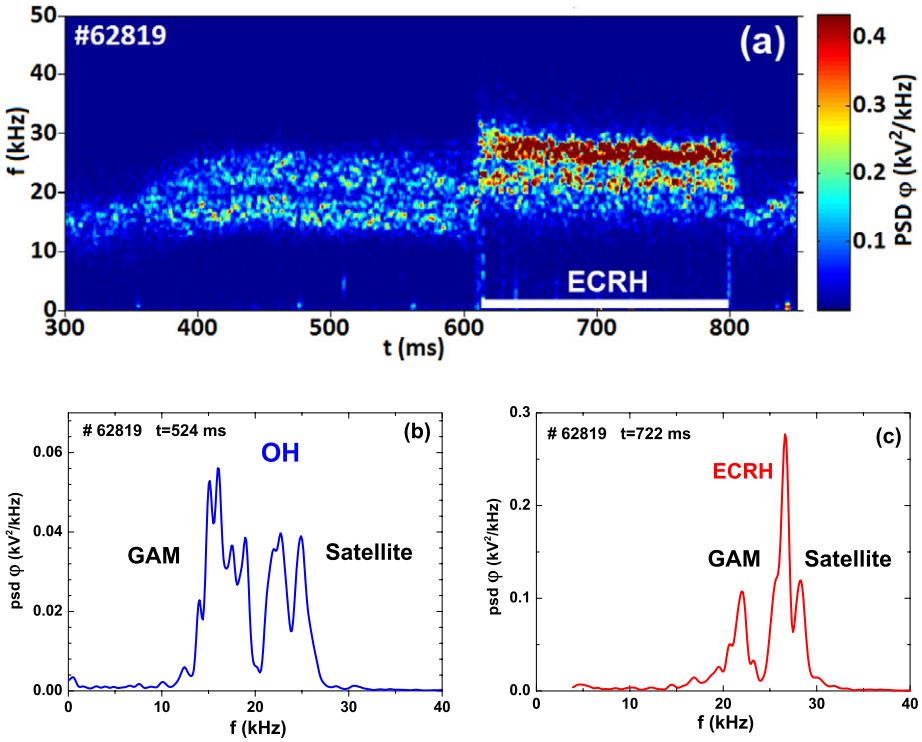

Figure 1. Spectrogram of potential perturbations in the discharge with Ohmic and auxiliary ECRH (*a*). Power density spectra in Ohmic (*b*) and ECRH (*c*) phases of discharge. $B_t = 2.27\,\mathrm{T}$, $I_\mathrm{p} = 200\,\mathrm{kA}$, $\bar{n}_\mathrm{e} = 2 \times 10^{19}\,\mathrm{m}^{-3}$, $\rho = 0.57$.

beam probing (HIBP) [12–14], correlation reflectometry and multipin Langmuir probes (MLPs) [15–17]. Previously our measurement in outer zone at the low field side have shown that the mode frequency f^exp scales approximately as $\sqrt{T}$ that confirms that these modes are induced by the geodesic compressibility and belong to the GAM/BAE type. The main goal of this work is to study the properties, radial and poloidal structure of such modes in the whole radial range and full operational limits of T-10.

2. Experimental observations of plasma potential oscillations associated to GAM

T-10 is a circular tokamak ($R = 1.5\,\mathrm{m}$, $a = 0.3\,\mathrm{m}$) with a rail carbon limiter. In this study a wide range of the plasma parameters was observed, from the lowest possible field $B_t = 1.55\,\mathrm{T}$ to the most typical $B_t = 2.42\,\mathrm{T}$. Plasma current was accordingly changed, covering the operational limits of T-10 from $I_\mathrm{p} = 140\,\mathrm{kA}$ to $I_\mathrm{p} = 330\,\mathrm{kA}$, while the edge safety factor q_a was changed from 4.2 to 2.54. The plasma line-averaged density evolves from the lowest possible values $\bar{n}_\mathrm{e} = 0.6\times10^{19}$ to $6\times10^{19}\,\mathrm{m}^{-3}$ due to the gas puffing from shot to shot and also during one shot. Two types of the gyrotrons with frequencies 129 and 140 GHz were used for on- and off-axis electron cyclotron resonance heating (ECRH) with total power P_EC up to 1.2 MW.

The main diagnostic tool for the presented study is HIBP [12, 14]. It operates on T-10 with Tl^+ probing beam, having energy E_b up to 280 keV. The probing region of HIBP (detector grid) was located in upper outer quadrant of plasma cross section at radii $0.06\,\mathrm{m} < r < 0.3\,\mathrm{m}$. HIBP operated in two main modes: (i) to measure the temporal potential evolution at a fixed point or (ii) to measure a potential profile by radial scan in the range 3–8 cm varying the entrance angle of probing beam each 10 ms. Radial profiles of the potential covering the full radial extension were obtained by a set of radial scans with different beam energies E_b in a series of identical discharges. The diagnostic set-up and the detector grid were described in figure 1 of our previous paper [18].

The GAM modes were observed in all types of the discharges; they are more pronounced on the potential than on the density. They are characterized by the main peak and the higher frequency satellite as presented in figure 1. We see that f^exp increases with T_e increase due to ECRH for both the main peak and the satellite.

2.1. GAM scaling on T_e

At first for comparison experiment with theory instead of (1) we use the simplified expression containing the dependence on T_e only and representing GAM:

$$f^\mathrm{e}_\mathrm{GAM} = \frac{1}{2\pi R}\sqrt{2T_\mathrm{e}/m_\mathrm{i}}. \qquad (2)$$

For the deuterium T-10 plasma with $R = 1.5\,\mathrm{m}$ it may be written as:

$$f^\mathrm{e}_\mathrm{GAM}[\mathrm{kHz}] = K\sqrt{T_\mathrm{e}\,[\mathrm{keV}]},\ K = 33. \qquad (2')$$

Experimental data shows that the observed main frequency peak f^exp follows the local GAM/BAE scaling with some reduction factor $\gamma(r)$: $f^\mathrm{exp} \sim \gamma(r) f^\mathrm{e}_\mathrm{GAM}$. This factor has maximum $\gamma \sim 1$ at $\rho = 0.7$ and decreases to the centre up to 0.5 and increases to the edge. So, one may suggest

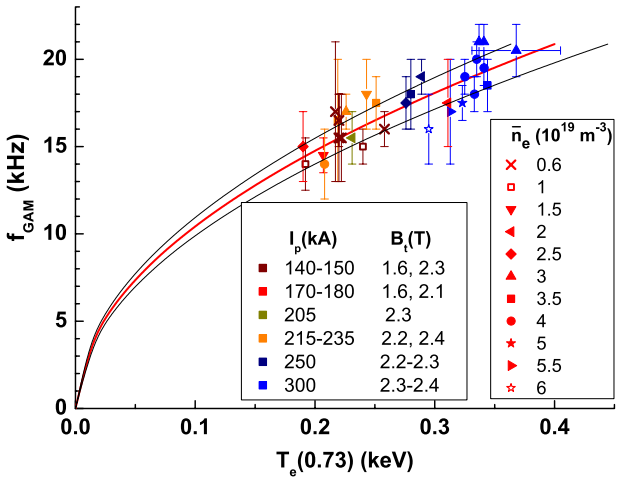

Figure 2. Dependence of GAM frequency on the electron temperature at the radius $\rho = 0.73$. Cumulative data over OH discharges with different currents 140 kA $< I_p <$ 300 kA marked by symbols of different colours and densities 0.6×10^{19} m^{-3} $< \bar{n}_e < 6 \times 10^{19}$ m^{-3}. Lines correspond to square root dependence (2′) with 10% variation of factor K. The typical error for T_e is 10%.

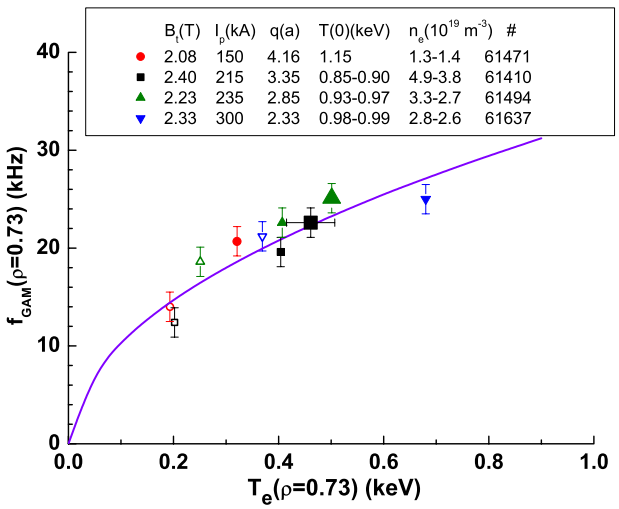

Figure 3. Dependence of GAM frequency on the electron temperature at the radius $\rho \approx 0.73$ for the discharges with OH and ECRH. Open symbols are OH, closed symbols are ECRH, small symbol shows the heating with one gyrotron, large symbol—with two gyrotrons. Lines correspond to square root dependence (2′). There is marked the typical 10% error for T_e.

that the observed GAM mode frequency is driven by the peripheral T_e ($\rho = 0.73$). Dependence of GAM frequency on the electron temperature at the radius $\rho = 0.73$ is shown in figure 2. It contains data over a wide range of Ohmic discharges with different currents 140 kA $< I_p <$ 300 kA and densities 0.6×10^{19} m^{-3} $< n_e < 6 \times 10^{19}$ m^{-3}. For the shots with unavailable T_e ($\rho = 0.73$) the data for the similar shots from T-10 database was taken according to [19]. Figure shows that $f^{exp} \sim f^{e}_{GAM}(0.73)$ when the local T_e varies widely within a factor of 2 over the whole set of the considered discharges, which covers whole operational limits of T-10.

Figure 3 presents the mode frequency versus T_e ($\rho = 0.73$) for the discharges with auxiliary ECRH. For the shots with

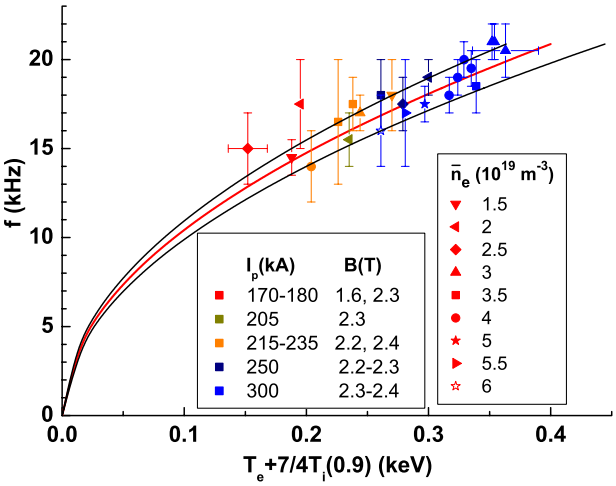

Figure 4. Dependence of GAM frequency on the electron and ion temperatures at the radius $\rho = 0.9$. Cumulative data over OH discharges with different currents 140 kA $< I_p <$ 300 kA and densities 0.6×10^{19} m^{-3} $< \bar{n}_e < 6 \times 10^{19}$ m^{-3} are marked by symbols of different sizes. Lines correspond to square root dependence (3) with 10% variation of f^{ei}_{GAM}. There are marked typical error bars for higher and lower temperatures, taken for 10% errors for T_e and 15% errors for T_i.

unavailable T_e ($\rho = 0.7$) at the ECRH phase, the modelling by the 1D transport code ASTRA was used. Figure 3 shows that $f^{exp} \sim f^{e}_{GAM}(0.73)$ with extended range of T_e variation up to the factor of 3.5. Since $q_a > 3$ in most of the experiments in T-10 we neglect the last term which is proportional to q^{-2} in equation (1):

$$f^{ei}_{GAM} = \frac{1}{\sqrt{2m_i}\pi R}\sqrt{T_e + 7/4T_i}. \qquad (3)$$

Ion temperature T_i was measured locally by CXRS [20]. The result presented in figure 4 shows that $f^{exp} \sim f^{ei}_{GAM}(0.9)$ in the wide range of the temperature variation (more than a factor of 2).

Finally, figures 2–4 shows that the observed mode follows the GAM temperature dependence. Moreover, for the whole observed operational limit of T-10 tokamak, the single value of $\rho = 0.9$ was found for the best fit for frequency.

2.2. Radial structure of GAM

The regimes with low magnetic fields allowing us to extend the HIBP observation area towards the plasma centre were studied in details. In these regimes HIBP was able to observe the area from the periphery ($\rho = 0.7$–1) to the centre ($\rho = 0.25$) and got the first indication of the radial constancy of the GAM frequency [10, 11]. Following [21] we study first the regime ($B_t = 1.55$ T, $I_p = 140$ kA), which is characterized by the low line-averaged density, slowly evolving from $\bar{n}_e = 1.3 \times 10^{19}$ to 2.4×10^{19} m^{-3} due to the gas-puffing. The time traces of the main plasma parameters are shown in figure 5. The central temperature $T_e(0)$ obtained with SXR-spectrograph slowly decreases and the absolute value of plasma potential φ strongly increases. At the lowest density, $\bar{n}_e = 1.3 \times 10^{19}$ m^{-3}, the modes are characterized by the main peak and the higher frequency satellite. The radial distribution of both peak and

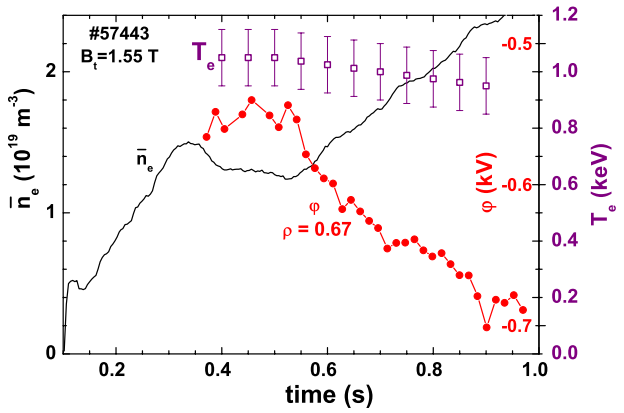

Figure 5. Evolution of plasma density $\bar{n}_e$, potential φ and electron temperature $T_e(0)$ in the regime with density ramp-up.

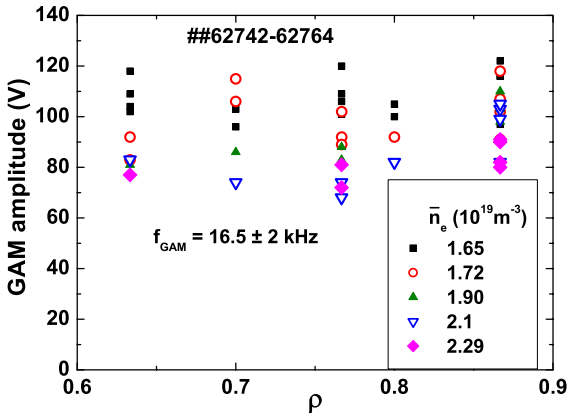

Figure 7. Radial dependence of GAM amplitude in regime with rising density measured by HIBP.

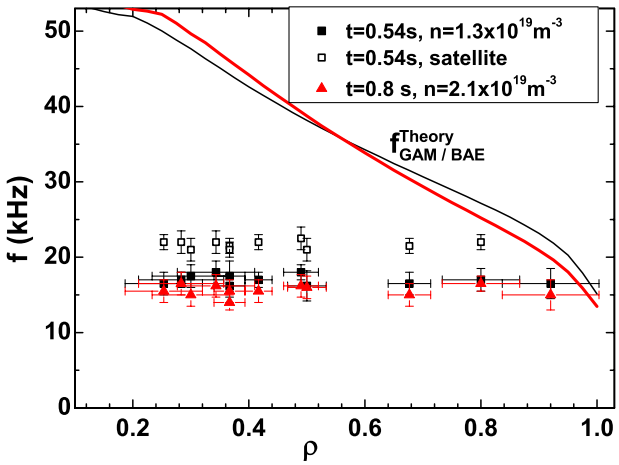

Figure 6. Radial distribution of GAM frequency, ■—$\bar{n}_e = 1.3 \times 10^{19}$ m^{-3}, ▲—$\bar{n}_e = 2.1 \times 10^{19}$ m^{-3}, closed symbols are the main peak, open symbols are satellites. The black thin line is calculated with equation (1) for $\bar{n}_e = 1.3 \times 10^{19}$ m^{-3} and the fat red line for $\bar{n}_e = 2.1 \times 10^{19}$ m^{-3}.

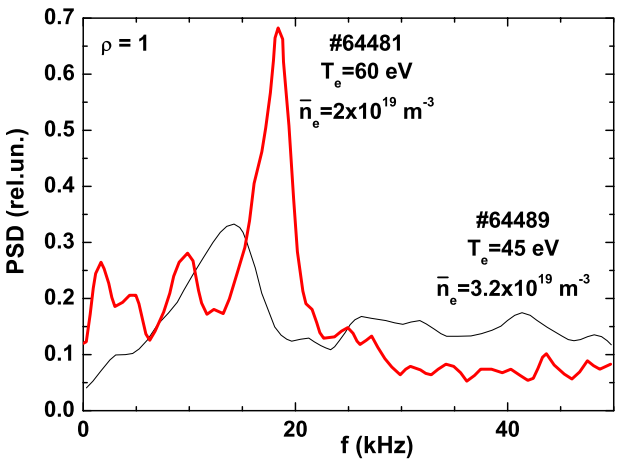

Figure 8. The power spectra of the edge potential oscillations measured by the Langmuir probe in shots with different temperatures and densities.

satellite is shown in figure 6; no modes were found at $\rho > 0.95$. The result shows the uniform structure of the mode: the mode frequency is close to a constant over the investigated interval ($0.2 < \rho < 0.9$), demonstrating inconsistency with equation (1) for f_{GAM} in the absolute value and radial shape. The constant mode frequency over the large radial extent suggests existence of the global eigenmode. Note, that the f^{exp} coincides with f_{GAM} only at the edge, at $\rho = 0.9$. With the density rise, the mode frequency is slightly decreasing, the satellite peak disappears at $\bar{n}_e \geqslant 2.1 \times 10^{19}$ m^{-3}. Later on, the main peak also disappears at $\bar{n}_e \geqslant 2.4 \times 10^{19}$ m^{-3}. At the edge, $\rho = 0.9$, slight decrease of f^{exp} happening with density rise is consistent with f_{GAM} prediction due to the evolution of the edge T_e and T_i.

2.3. GAM dependence on density

GAM amplitude evolution with density increase was first studied by HIBP at the plasma periphery [22]. In the present study the wide radial area was analysed for the first time. Figure 7 shows the radial distribution of the GAM peak in another series of shots with the density variation. We see that GAM amplitude is almost constant over a wide radial zone and decreases/increases with density rise/fall-down. Above mentioned dependencies of GAM frequency on the electron temperature and density agrees with data of MLP are presented in figure 8. We see that at the plasma edge, $\rho = 1$, the peak in GAM frequency range is clearly seen. The peak frequency increases with T_e increase and its amplitude decreases with the density increase. Here T_e was measured locally by Langmuir probe.

2.4. GAM evolution in the discharges with current ramp-up

The time traces of the main plasma parameters in another regime with $B_t = 2.08$ T, $\bar{n}_e = 2.5 \times 10^{19}$ m^{-3},the current ramp-up from $I_p = 160$ kA to $I_p = 212$ kA and off-axis ECRH ($\rho_{\mathrm{ECRH}} = 0.5$, $P_{\mathrm{EC}} = 0.9$ MW) are shown in figure 9. The time evolution of the GAM frequency near the plasma centre is shown in lower box of figure 9. The mode frequency is evolving with T_e rise due to the ECRH and the increase of the OH power due to the current ramp-up. It scales with T_e as predicted by equation (1) for f_{GAM}, and consistent with the absolute values of frequency within a factor of 0.5. The radial distribution of f^{exp} is shown in figure 10. Similar to the regime with $B_t = 1.55$ T shown in figures 5 and 6, we see the

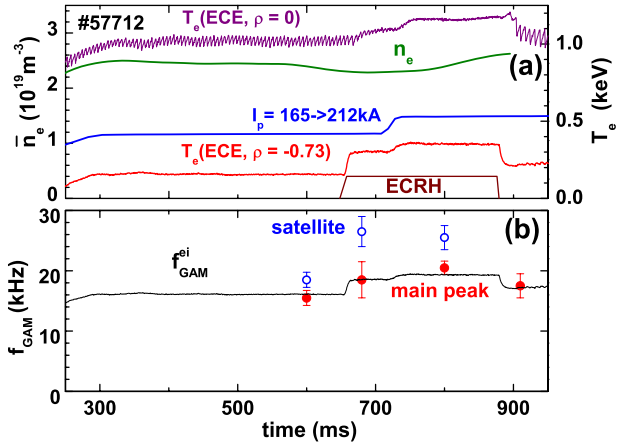

Figure 9. (*a*) Time traces of line-averaged density, plasma current and electron temperature in the regime with current ramp-up and ECRH; (*b*) time evolution of the GAM frequency $f^{\exp}$ for the main peak (full circles) and satellite (open circles). The error bars denote the width of the frequency peaks; $\cdot f^{\rm ei}_{\rm GAM}(\rho = 0.9)$ is shown by the black curve.

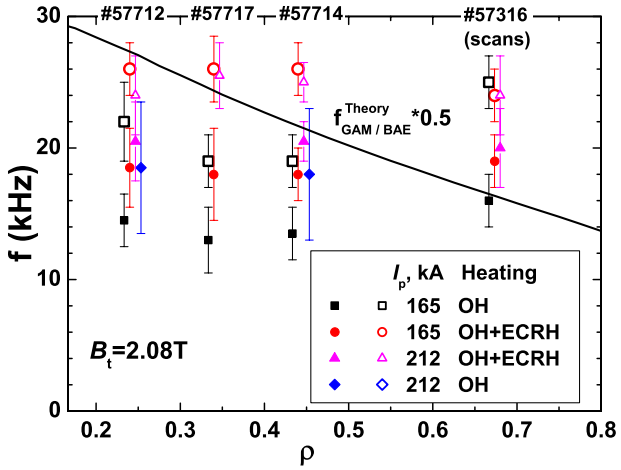

Figure 10. Radial distribution of the GAM frequency peak for four stages of the discharge from figure 9. Full symbols are main peaks, open symbols are satellites. Points in each group are radially shifted a bit for clearance. The black line is 0.5 $f^{\rm ei}_{\rm GAM}(\rho)$ for OH, $I_{\rm p} = 165$ kA.

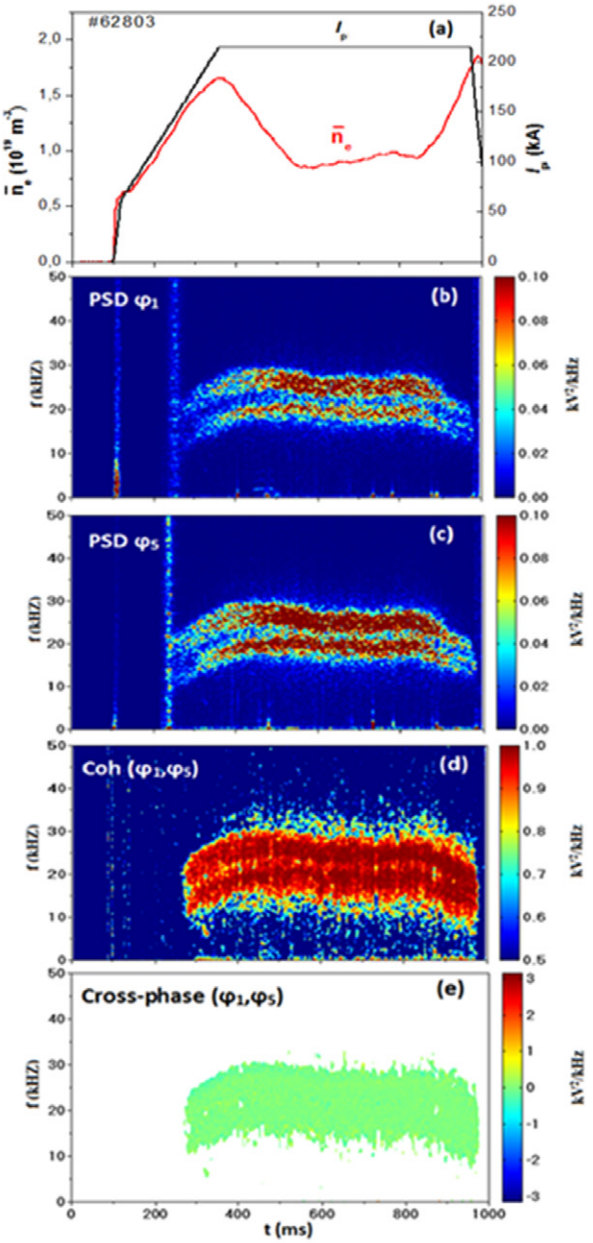

Figure 11. Traces of plasma current $I_{\rm p}$ and line-averaged plasma density $\bar{n}_{\rm e}$ (*a*); power spectral densities of potential oscillations measured in two most distant sample volumes by the upper slit φ_1 (*b*) and lower slit φ_5 (*c*) with the 5-slit HIBP energy analyser at radius $r = 21$ cm, $B_t = 2.3$ T, their coherency (*d*) and cross-phase (*e*). The cross-phase is shown for the points with high coherency, coh $(\varphi_1, \varphi_5) > 0.8$.

same uniform radial structure: the mode frequency is constant over the investigated interval, showing the feature of the global eigenmode. No GAM frequency dependence on the toroidal field B_t is observed.

2.5. GAM poloidal structure

For determination of the GAM poloidal structure we used the two-point correlation method [23]. The method is based on calculation of phase shift θ between GAMs measured by HIBP simultaneously in two sample volumes, separated poloidally at the same magnetic surface. The phase shift between signals is linked with the poloidal mode number m and the poloidal angle between two sample volumes α as follows: $m = \theta/\alpha$ [24]. Figure 11 presents the results of analysis for the typical shot together with time traces of discharge current $I_{\rm p}$ and line-averaged density $\bar{n}_{\rm e}$. Figure shows that both signals from poloidally shifted sample volumes are very similar. We see the main peak and high-frequency satellite with frequencies about 20 kHz slightly evolving with density. They have rather good coherency, coh > 0.8, and their cross-phase is near zero. This means that $m = 0$.

The similar results were obtained for other couples of sample volumes and for different discharges. Finally, poloidal mode numbers are near zero, $m = 0$, over the whole radii within the achieved experimental accuracy as presented in figure 12.

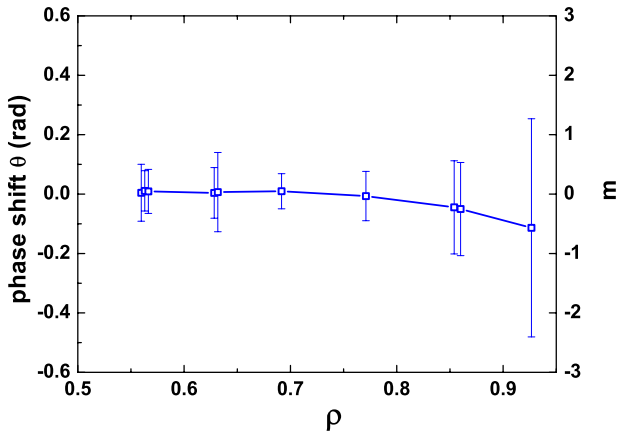

Figure 12. The phase shift between the potential oscillations and the poloidal mode number m measured by intermediate slits of the analyser. Discharge parameters $B_t = 2.3$ T, $\bar{n}_e = (0.9\text{–}2.4) \times 10^{19}$ m^{-3}, $I_p = 220$ kA, Ohmic heating.

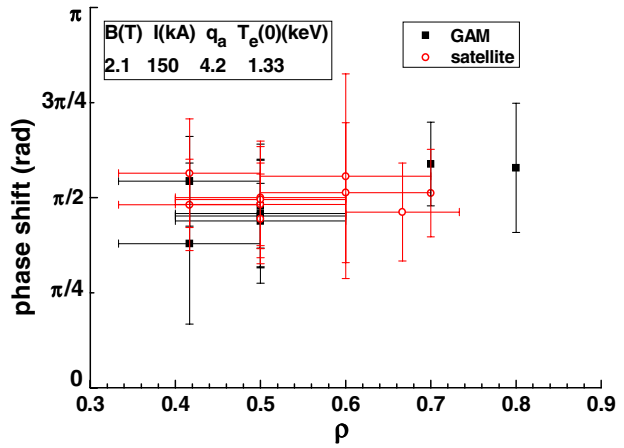

Figure 13. Phase shift between oscillations of potential and density for the main GAM peak and satellite in the Ohmic regime ($B_t = 2.1$ T, $I_p = 150$ kA, $q_a = 4.2$, $T_e(0) = 1.3$ keV). Horizontal bars denote the swings of the HIBP scan.

2.6. Relations between potential and density oscillations

The phase shift between density and potential oscillations for the main GAM peak and satellite is equal to $\pi/2 \pm 0.15\pi$ (figure 13). The ratio between relative amplitude of the potential and density oscillations (Boltzmann ratio) for the considered regimes is $e\delta\varphi/T_e = k\delta n_e/n_e$ with $k \sim 10$–60 that differs from electrostatic drift broadband turbulence which usually shows $k \sim 1$.

3. Discussion

Theoretically the global eigenmode can occur, if f_{GAM} profile has a local maximum [25]. This is not the case of the experiments in the modern tokamaks where the local GAM frequency is monotonic as in figure 6. Some recent theoretical results [26, 27] predict the global GAMs in discharges with positive magnetic shear and monotonic temperature profile. However, in this theory the mode originates from the centre, while in our experiment the mode seems to be excited at the edge.

The radial constancy or weak radial dependence of GAM frequency was observed on several fusion devices (JFT-2M [8], ASDEX-U [9], JIPP-TIIU [28], HL-2A [29], TCV [30]), while on FT-2 [7] and Globus-M tokamaks [31] the GAM frequency smoothly increases towards the centre. However these studies of the radial structure of GAM were limited by the diagnostic capabilities. The HIBP measurement in JFT-2M [8], were possible for the plasma periphery. GAM potential perturbation manifested itself like a radially propagating wave from the core to the edge. Both narrow and broad spectra of GAMs with different intensity were observed by HIBP in plasma potential over almost the whole plasma cross section in regimes with different methods of heating (neutral beam injection (NBI) and ion cyclotron resonance frequency (ICRF) or OH correspondingly) at the JIPP-TIIU tokamak [28, 32]. The authors report the unexpected frequency decrease with the temperature raise at the auxiliary heating phase of the discharge and show the radial uniformity of the mode frequency similar to our results. Experiments on DIII-D observed GAMs with a constant frequency and narrow spectral peak in the edge region $\rho > 0.86$ only [33].

In the present paper we report the radial uniformity of the mode frequency and amplitude of plasma potential measured by HIBP over almost the whole radial interval. This data were supported with the edge measurements at $\rho = 1$ by MLPs, which observed the pronounced GAM peak on the floating potential and tiny peak in the ion saturation current reflecting plasma density. This data were also supported in the core region with the correlation reflectometry measurements of the GAM associated density perturbation at $\rho = 0.1$ [34]. Remarkably, the GAM frequency is constant over the whole radial interval from the centre to the edge. The absolute value of the GAM frequency coincides with the local formula (3) for the $\rho = 0.9$. The measurements of three diagnostics are consistent to each other. The evidence of the long-range (1/4 of the torus) toroidal correlations between the HIBP potential and density, measured by correlation reflectometry, supports the global character of the GAM [21, 35]. The radial correlation length exceeds few cm [36], pointing out to the nonlocal GAM eigenmode. This is in agreement with nonlocal GAMs simulations [37] which show a mesoscopic global mode with the radial extent of the order $\sqrt{a\rho_i}$, and where the mode frequency remains constant over the wide radial extent bound by the local GAM and ion sound continua. Several extended plateau regions exhibiting the uniform frequency in each region were also reported in [9] and numerical simulations of [38].

The GAM may be excited by several mechanisms that were suggested in the literature such as drift wave turbulence [39], energetic particles [40] or electron current [41]. The excitation mechanism will also compete against damping due to Landau damping [42] and ion-ion collisions [43]. The collisional damping related to ion viscosity may be responsible for GAM suppression with raising density.

The basic GAM mode consists of $m = 0$ and $m = 1$ potential fluctuations and $m = 1$ density fluctuations. There is negligible density fluctuations in $m = 0$ component. The amplitude of the $m = 1$ potential fluctuations is smaller than the $m = 0$ component, $\phi_1 \sim k_r\rho_i\phi_0$. The $m = 1$ density perturbation is related to the $m = 0$ potential by the relation

$-\mathrm{i}\omega n_1 - 2n_0 c/B_0(\partial\varphi_0/\partial r)(\partial/\partial\theta)\ln B_0 = 0$. Assuming $\phi_0 \sim \exp(-\mathrm{i}\omega t + \mathrm{i}k_r r)$ one has $-\omega n_1 - 2n_0 c/B_0 k_r \varphi_0(\partial/\partial\theta)\ln B_0 = 0$ which means the absence of the phase shift between the density and $m = 0$ potential for the real k_r. The observed $\pi/2$ phase shift may suggest the imaginary k_r, or equivalently the standing wave of the global mode trapped between local GAM and sound continua. However, the picture of the standing mode is not fully consistent with the uniformity of the GAM amplitude observed in our experiments: one can expect that the amplitude of radially propagating wave packet will change due to energy conservation in cylindrical geometry of the $m = 0$ mode.

It has been shown that the experimental GAM frequency and amplitude is constant over the radius and absolute value of the experimental GAM frequency coincides with the theoretical expectation (3) at $\rho = 0.9$. These observation may suggest that the observed GAM global mode is driven by the drift wave turbulence at the periphery and then extends globally from the source region $\rho = 0.9$ to both sides in radial direction, toward the plasma centre as well as the edge. Such view is consistent with the observations reported in the paper. The radial propagation of GAMs were previously reported in JFT-2M [8] and TCV [30]. The radial profile of the GAM amplitude is likely a result of combined GAM propagation and location of energy sources/sinks [28, 32]. The features of the radial propagation of potential perturbations in the T-10 tokamak are topic for the future study.

4. Summary

On T-10 the modes in the geodesic acoustic frequency range are found to be present in the plasma potential and density. They are typically observed as a main peak, accompanied by a higher frequency satellite in some cases as also reported in [9, 16]. The modes are more pronounced during ECRH rather than OH. The typical frequencies are seen in the band from 12–20 kHz in OH and 22–30 kHz in ECRH over the whole plasma cross-section suggesting the features of the global eigenmode. The poloidal mode number on potential is $m = 0$ as predicted by GAM theory. The frequency of the mode does not show dependence on the magnetic field and plasma density, but the amplitude decreases with density rise indicating the GAM collisional damping. The phase shift between the oscillations on potential and density is about $\pi/2$. The absolute value of the mode frequency is consistent with f_{GAM} scaling at the edge, $f \sim \sqrt{T(\rho = 0.9)}$, indicative this mode is the edge driven eigenmode. Finally, the features of the GAM as a nonlocal (global) eigenmode were observed.

Acknowledgments

The experimental results of sections 2.1–2.3 and 2.5–2.6 were obtained due to the funding of Russian Science Foundation, project 14-22-00193.

References

[1] Fujisawa A. *et al* 2007 Experimental progress on zonal flow physics in toroidal plasmas *Nucl. Fusion* **47** S718
[2] Winsor N. *et al* 1968 Geodesic acoustic waves in hydromagnetic systems *Phys. Fluids* **11** 2448
[3] Heidbrink W.W. *et al* 1999 What is the beta-induced Alfvén eigenmode? *Phys. Plasmas* **6** 1147
[4] Zonca F. and Chen L. 2008 Radial structures and nonlinear excitation of geodesic acoustic modes *Europhys. Lett.* **83** 35001
[5] Smolyakov A.I. *et al* 2010 Electromagnetic effects on geodesic acoustic and beta-induced Alfvén eigenmodes *Nucl. Fusion* **50** 054002
[6] Smolyakov A.I., Garbet X., Falchetto G. and Ottaviani M. 2008 Multiple polarization of geodesic curvature induced modes *Phys. Lett.* A **372** 6750
[7] Gurchenko A.D. *et al* 2013 Spatial structure of the geodesic acoustic mode in the FT-2 tokamak by upper hybrid resonance Doppler backscattering *Plasma Phys. Control. Fusion* **55** 085017
[8] Ido T. *et al* 2006 Geodesic–acoustic-mode in JFT-2M tokamak plasmas *Plasma Phys. Control. Fusion* **48** S41
[9] Conway G. 2008 Frequency scaling and localization of geodesic acoustic modes in ASDEX Upgrade *Plasma Phys. Control. Fusion* **50** 055009
[10] Melnikov A.V. *et al* 2010 Study of geodesic acoustic induced modes in T-10 tokamak *Proc. 37th EPS Conf. on Plasma Physics (Ireland, OH, 21–25 June 2010)* vol 34A (ECA) P1.056 (http://ocs.ciemat.es/EPS2010PAP/pdf/P1.056.pdf)
[11] Melnikov A.V. *et al* and The HIBP Team 2013 Radial mode structure of plasma fluctuations in the GAM frequency range in OH and ECRH plasmas on the T-10 tokamak *Proc. 40th EPS Conf. on Plasma Physics (Espoo, Finland, 1–5 July 2013)* vol 37D (ECA) P. 2.178 (http://ocs.ciemat.es/EPS2013PAP/pdf/P2.178.pdf)
[12] Melnikov A.V. *et al* 1995 HIBP diagnostics on T-10 1995 *Rev. Sci. Instrum.* **66** 317
[13] Melnikov A.V. *et al* 1994 Space and time evolution of plasma potential in T-10 under variation of main gas influx *IEEE Trans. Plasma Sci.* **22** 363
[14] Donné A.J.H. *et al* 2002 Diagnostics for radial electric field measurements in hot magnetized plasma *Czech. J. Phys.* **52** 1077
[15] Melnikov A.V. *et al* 2005 Investigation of the plasma potential oscillations in the range of geodesic acoustic mode frequencies by heavy ion beam probing in tokamaks *Czech. J. Phys.* **55** 349
[16] Melnikov A.V. *et al* 2006 Investigation of geodesic acoustic mode oscillations in the T-10 tokamak *Plasma Phys. Control. Fusion* **48** S87
[17] Melnikov A.V. *et al* 2011 Plasma potential and turbulence dynamics in toroidal devices (survey of T-10 and TJ-II experiments) *Nucl. Fusion* **51** 083043
[18] Melnikov A.V. *et al* 2013 Electric potential dynamics in OH and ECRH plasmas in the T-10 tokamak *Nucl. Fusion* **53** 093019
[19] Kirneva N.A. *et al* 2014 Empirical formula for plasma electron temperature profile in T-10 ohmic discharges *Prob. At. Sci. Technol.* **37** 56 (in Russian)
[20] Klyuchnikov L.A. *et al 2014* Impurities removal during central ECR heating in T-10 *Proc. 25th IAEA Fusion Energy Conf. (St. Petersburg, Russia, 13–18 October 2014)* EX/P1-44 www-pub.iaea.org/iaeameetings/46091/25th-Fusion-Energy-Conference-FEC-2014
[21] Melnikov A.V. *et al* 2014 Radial homogeneity of the geodesic acoustic modes in the ohmic discharges with low B in the T-10 tokamak *JETP Lett.* **100** 555–60
[22] Melnikov A.V. *et al 2008* Study of correlation properties of geodesic acoustic modes in the T-10 Tokamak *Proc. 22nd IAEA Fusion Energy Conf. (Geneva, Switzerland, 13–18 October 2008)* EX/P5-36 (www-naweb.iaea.org/napc/physics/FEC/FEC2008/papers/ex_p5-36.pdf)
[23] Eliseev L.G. *et al* 2012 Two point correlation technique for the measurements of poloidal plasma rotation by heavy ion beam probe *Plasma Fusion Res.* **7** 2402064
[24] Zenin V.N., Eliseev L.G., Kozachek A.S., Krupnik L.I., Lysenko S.E., Melnikov A.V. and Perfilov S.V. 2014 Study

of poloidal structure of geodesic acoustic modes in the T-10 tokamak with heavy ion beam probing *Prob. At. Sci. Technol.* **6** 269
[25] Berk H.L., Boswell C.J., Borba D., Figueiredo A.C.A., Johnson T., Nave M.F.F., Pinches S.D. and Sharapov S.E. 2006 Explanation of the JET $n = 0$ chirping mode *Nucl. Fusion* **46** S888
[26] Ilgisonis V.I. *et al* 2013 Global geodesic acoustic mode in a tokamak with positive magnetic shear and a monotonic temperature profile *Plasma Phys. Control. Fusion* **56** 035001
[27] Ilgisonis V.I. *et al* 2014 Analytical solutions for global geodesic acoustic modes in tokamak plasmas *Plasma Phys. Rep.* **40** 843
[28] Hamada Y. *et al* 2011 Detection of the kinetic geodesic acoustic mode (KGAM) near the centre region of JIPPT-IIU tokamak plasmas *Nucl. Fusion* **51** 033005
[29] Chen W. *et al* 2013 Observation of energetic-particle-induced GAM and nonlinear interactions between EGAM, BAEs and tearing modes on the HL-2A tokamak *Nucl. Fusion* **53** 113010
[30] de Meijere C.A. *et al* 2014 Complete multi-field characterization of the geodesic acoustic mode in the TCV tokamak *Plasma Phys. Control. Fusion* **56** 072001
[31] Yashin A.Yu. *et al* 2014 Geodesic acoustic mode observations in the Globus-M spherical tokamak *Nucl. Fusion* **54** 114015
[32] Hamada Y. *et al* 2012 Regions of kinetic geodesic acoustic modes and streamers in JIPPT-IIU tokamak plasmas *Nucl. Fusion* **52** 063023
[33] Hillesheim J.C., Peebles W.A., Carter T.A., Schmitz L. and Rhodes T.L. 2012 Experimental investigation of geodesic acoustic mode spatial structure, intermittency, and interaction with turbulence in the DIII-D tokamak *Phys. Plasmas* **19** 022301
[34] Shelukhin D.A., Vershkov V.A. and Khmara A.V. 2008 Spatial structure of density fluctuations and geodesic acoustic mode in T-10 tokamak *Proc. 22nd IAEA Fusion Energy Conf. (Geneva, Switzerland, 13–18 October 2008)* EX/P5-37 www-naweb.iaea.org/napc/physics/FEC/FEC2008/papers/ex_p5-37.pdf
[35] Melnikov A.V. *et al* Correlation properties of geodesic acoustic modes in the T-10 Tokamak *J. Phys. Conf. Ser.* **591** 012003
[36] Melnikov A.V. *et al* 2015 Long-distance correlations of geodesic acoustic modes in T-10 *Prob. At. Sci. Technol.* **38** 49 (in Russian)
[37] Miyato N., Kishimoto Y. and Li J.Q. 2006 Nonlocal behaviour of zonal flows in tokamak plasmas *Plasma Phys. Control. Fusion* **48** A335
[38] Robinson J.R., Hnat B., Thyagaraja A., McClements K.G., Knight P.J. and Kirk A. 2013 Global two-fluid simulations of geodesic acoustic modes in strongly shaped tight aspect ratio tokamak plasmas *Phys. Plasmas* **20** 052302
[39] Chakrabarti N. *et al* 2007 Nonlinear excitation of geodesic acoustic modes by drift waves *Phys. Plasmas* **14** 052308
[40] Zarzoso D. *et al* 2013 Impact of energetic-particle-driven geodesic acoustic modes on turbulence *Phys. Rev. Lett.* **110** 125002
[41] Elfimov A.G., Smolyakov A.I. and Galvao R.M.O. 2014 Geodesic mode instability driven by the electron current in tokamak plasmas *Phys. Lett.* A **378** 800
[42] Watari T., Hamada Y., Notake T., Takeuchi N. and Itoh K. 2006 Geodesic acoustic mode oscillation in the low frequency range *Phys. Plasmas* **13** 062504
[43] Smolyakov A.I. 2014 Elements of neoclassical theory and plasma rotation in a tokamak *Rotation and Momentum Transport in Magnetized Plasmas* ed P. Ghendrich (Singapore: World Scientific)